Temperature dependences of the electron–phonon coupling, electron heat capacity and thermal conductivity in Ni under femtosecond laser irradiation

Zhibin Lin, Leonid V. Zhigilei *

Department of Materials Science and Engineering, University of Virginia, 116 Engineer's Way, Charlottesville, VA 22904-4745, USA

Abstract

The electron temperature dependences of the electron–phonon coupling factor, electron heat capacity and thermal conductivity are investigated for Ni in a range of temperatures typically realized in femtosecond laser material processing applications, from room temperature up to temperatures of the order of 10^4 K. The analysis is based on the electronic density of states obtained through the electronic structure calculations. Thermal excitation of d band electrons is found to result in a significant decrease in the strength of the electron–phonon coupling, as well as large deviations of the electron heat capacity and the electron thermal conductivity from the commonly used linear temperature dependences on the electron temperature. Results of the simulations performed with the two-temperature model demonstrate that the temperature dependence of the thermophysical parameters accounting for the thermal excitation of d band electrons leads to higher maximum lattice and electron temperatures achieved at the surface of an irradiated Ni target and brings the threshold fluences for surface melting closer to the experimentally measured values as compared to the predictions obtained with commonly used approximations of the thermophysical parameters.

1. Introduction

The fast growth of femtosecond laser applications has increased the demand for realistic computational description of highly nonequilibrium processes induced in a target material by the fast laser energy deposition. The time evolution of the electron and lattice temperatures in a metal target irradiated by a femtosecond laser pulse is commonly described by the two-temperature model (TTM) [1], that accounts for the laser energy absorption by the conduction band electrons, energy transfer from hot electrons to the atomic vibrations due to the electron–phonon coupling, and the electronic heat diffusion from the irradiated surface to the bulk of the target.

The accuracy of a quantitative description of the kinetics of energy redistribution in the irradiated target in a big part relies on the appropriate choice of the temperature dependent thermophysical properties of the target material included in the TTM equations, namely, the electron–phonon coupling factor, the electron heat capacity and the heat conductivity. Due to the small electron heat capacity of the electrons, the electron temperature in the surface region of the irradiated target can be transiently brought to very high values, comparable to the Fermi temperature. At such high electron temperatures, T_e, the temperature dependent thermophysical properties of noble [2–5] and transition metals [5] can be directly affected by the thermal excitation of the lower band electrons.

The effect of the thermal excitation of electrons on the thermophysical properties is sensitive to the details of the electronic structure of the target material. In particular, in Au the d band lies ∼2 eV below the Fermi level and at T_e below

---

* Corresponding author. Tel.: +1 434 243 3582; fax: +1 434 982 5660.
  E-mail addresses: zl5c@virginia.edu (Z. Lin), lz2n@virginia.edu
(L.V. Zhigilei).

$\sim$3000 K ($\sim$0.25 eV) the d band electrons do not contribute to the electron–phonon coupling and the electron heat capacity, whereas at $\sim$10^4 K ($\sim$1 eV) thermal excitation of d band electrons results in a significant increase of both the electron–phonon coupling factor and the electron heat capacity (e.g. the electron–phonon coupling factor exceeds the room temperature value by a factor of 8.9 at $T_e = 2 \times 10^4$ K [4]). On the other hand, in transition metals, such as Ni or Pt, the Fermi level cuts through the d band, resulting in a very high density of electron states at the Fermi level. In this case, the thermal excitation of electrons from high density of states d band to the low density of states s band can have the opposite effect on the electron heat capacity and electron–phonon coupling as compared to noble metals. In particular, the electron heat capacity of Pt has been shown to become smaller than the value given by the linear dependence on the electron temperature predicted by the Sommerfeld expansion for the electronic free energy [5]. Therefore, a detailed analysis of the connections between the electron density of states (DOS) in the target material and the temperature dependence of the thermophysical material properties is needed for a realistic description of laser material interactions.

In this paper, we investigate the effect of the thermal excitation of the d band electrons on the thermophysical properties of Ni. In the next section, the connections between the electron DOS of Ni and the temperature dependence of the electron–phonon coupling, electron heat capacity and thermal conductivity are analyzed. The qualitative differences between the temperature dependences obtained for Ni and earlier predictions for Au [4] are related to the differences in the electron DOS of the two metals. In Section 3, practical implications of the thermal excitation of the d band electrons are investigated by performing a series of TTM simulations with the modified temperature-dependent thermophysical properties. The evolution of the kinetics of the electron–phonon equilibration, the electron and lattice temperatures, and the fluence thresholds for surface melting are investigated for Ni films of various thicknesses and a bulk Ni target. A brief summary of the results is given in Section 4.

2. The effect of thermal excitation of electrons on thermophysical properties of Ni

The effect of the thermal excitation of electrons on thermophysical properties of Ni is investigated here based on the electron DOS obtained from the electronic structure calculation performed within the density functional theory using the Vienna Ab-initio Simulation Package (VASP) [6]. The Projector Augmented Wave (PAW) potential [7] is used in the calculation, where the exchange correlation term is treated within the Generalized Gradient Approximation (GGA). The calculations are done for nonmagnetic Ni at the equilibrium lattice constant of 3.53 Å. The electron DOS for Ni obtained from VASP at $T_e = 0$ K is shown in Fig. 1, together with the Fermi distribution function plotted at three different values of the electron temperature.
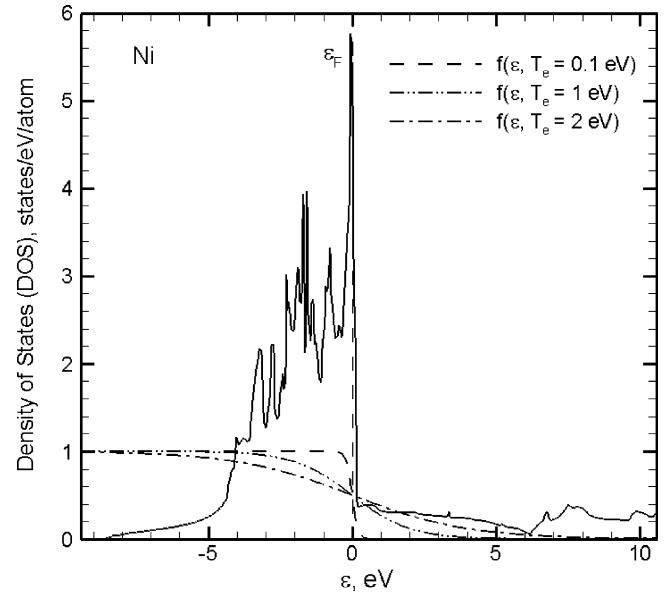

Fig. 1. Electron DOS of Ni obtained in electron structure calculations performed with VASP (solid line). The Fermi distribution function is also shown for three different values of the electron temperature. The energy is shown with respect to the Fermi level at zero temperature, ε_F.

The electron heat capacity dependence on the electron temperature can be expressed as [8]:

$$C_e(T_e) = \int_{-\infty}^{\infty} (\varepsilon - \varepsilon_F) \frac{\partial f(\varepsilon, \mu, T_e)}{\partial T_e} g(\varepsilon) \, d\varepsilon \qquad (1)$$

where $g(\varepsilon)$ is the electron DOS at the energy level ε, μ the chemical potential at T_e and $f(\varepsilon, \mu, T_e)$ is the Fermi distribution function, defined as $f(\varepsilon, \mu, T_e) = \{\exp[(\varepsilon - \mu)/k_B T_e] + 1\}^{-1}$. The determination of the chemical potential μ, required in Eq. (1), is done through setting the result of the integration of the product of DOS and the Fermi distribution function at T_e over all energy levels to be equal to the total number of valence electrons. It can be seen from Figs. 1 and 2(a) that as the electron temperature increases, the excitation from high density of states below ε_F to the states above ε_F increases, leading to the increase in the chemical potential, whereas the chemical potential of the free electron model, calculated from the Sommerfeld expansion at low temperatures [8], decreases.

In Fig. 2(b), the temperature dependence of the electron heat capacity, calculated from Eq. (1) with the DOS determined from VASP calculations, is shown together with the commonly used linear approximation, $C_e(T_e) = \gamma T_e$, obtained from the Sommerfeld expansion with $\gamma = 1065$ J m^{-3} K^{-2} measured at low temperatures [9]. The heat capacity calculated with the realistic DOS is lower than the one predicted by the linear dependence, $C_e(T_e) = \gamma T_e$, at all temperatures and exhibits a steadily increasing deviation from the linear dependence. This deviation can be explained by analyzing the characteristics of the Ni DOS shown in Fig. 1. The high density of electron states at the Fermi level ensures that the 3d band electrons can be easily excited to the 4s band. The 4s band has a much smaller density of states as compared to the density of states at the
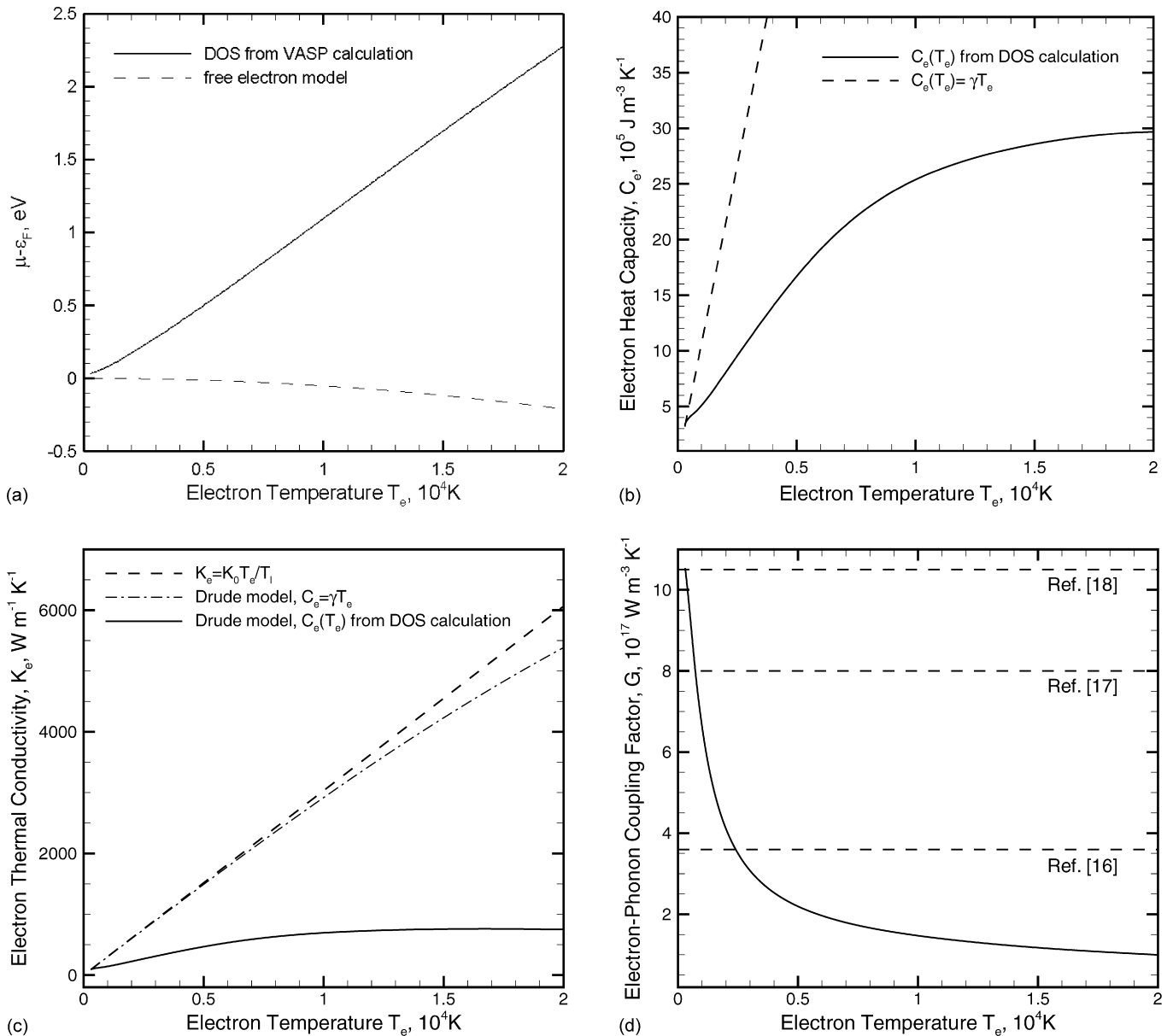
Fig. 2. Electron temperature dependences of thermophysical properties of Ni. Solid lines show the results of the calculations performed with DOS obtained from VASP. Dashed lines show the commonly used approximations of the thermophysical material properties. Chemical potential is shown in (a), electron heat capacity in (b), electron thermal conductivity in (c) and electron–phonon coupling factor in (d). Data presented in this figure are accessible in tabulated form from Ref. [11].

Fermi level, leading to the negative deviation of the heat capacity from the linear dependence, which is obtained from the Sommerfeld expansion at a low electron temperature. This behavior of the heat capacity is similar to the one reported for Pt [5], which has the electron DOS similar to Ni, but different from Au, where the thermal excitation from the low-laying d band results in the positive deviation of the heat capacity from the linear dependence at sufficiently high electron temperatures [4,5]. The trend of the negative deviation of the electron heat capacity from the linear dependence shown in Fig. 2(b) agrees with the results reported for Ni in Ref. [10], where the electronic heat capacity was obtained by subtracting the lattice heat capacity (assumed to follow the Dulong–Petit law at high temperatures), from the total heat capacity measured in experiments for temperatures up to 1600 K.

The electron thermal conductivity is directly affected by the thermal excitation of d band electrons as it is related to the electron heat capacity through the Drude model relationship, $K_e(T_e, T_l) = v_F^2 C_e(T_e)\tau_e(T_e, T_l)/3$ [8], where v_F is the Fermi velocity and $\tau_e(T_e, T_l)$ is the total electron scattering time. The total electron scattering time is defined by the electron–electron scattering time, τ_{e-e}, and the electron–phonon scattering time, τ_{e-ph}, and can be evaluated from the sum of the scattering rates, $1/\tau_e = (1/\tau_{e-e}) + (1/\tau_{e-ph}) = AT_e^2 + BT_l$, where $A = 1.4 \times 10^6 \text{ K}^{-2} \text{ s}^{-1}$ and $B = 1.624 \times 10^{13} \text{ K}^{-1} \text{ s}^{-1}$ for Ni [12]. Fig. 2(c) shows the electron thermal conductivity calculated with three different approximations, namely, a linear dependence on the electron temperature neglecting the contribution from the electron-electron scattering, $K_e = K_0 T_e/T_l$ with $K_0 = 91 \text{ W m}^{-1} \text{ K}^{-1}$ [9], Drude model with $C_e(T_e) = \gamma T_e$, and

Drude model with $C_e(T_e)$ evaluated from Eq. (1) using the DOS calculated with VASP. It is clear from Fig. 2(c) that the deviation of the heat capacity from the linear dependence, Fig. 2(b), will also result in slower electron heat conduction, especially at the early stage of the electron–phonon equilibration, when the electron temperature is close to its maximum.

In the analysis of the electron temperature dependence of the electron–phonon coupling factor we follow the approach suggested in Refs. [2,13] and applied earlier for the analysis of the temperature dependence of the electron–phonon coupling in Au [2–4]. Within this approach, the electron–phonon coupling factor accounting for the thermal excitation of electrons from the energy levels located below the Fermi level can be expressed as [2]:

$$G(T_e) = \frac{\pi \hbar k_B \lambda \langle \omega^2 \rangle}{g(\varepsilon_F)} \int_{-\infty}^{\infty} g^2(\varepsilon) \left(-\frac{\partial f}{\partial \varepsilon} \right) d\varepsilon \qquad (2)$$

where λ is the electron–phonon coupling constant used in the superconductivity theory and $\langle \omega^2 \rangle$ is the second moment of the phonon spectrum defined by McMillan [14]. At low electron temperatures, $-\partial f/\partial \varepsilon$ reduces to a delta function and Eq. (2) yields the expression proposed by Allen: $G_0 = \pi \hbar k_B \lambda \langle \omega^2 \rangle g(\varepsilon_F)$ [13], featuring a constant value. Using $\lambda = 0.084$ for Ni [15] and an approximation for $\langle \omega^2 \rangle = 1/2\theta_D^2$ [14,15], where $\theta_D = 450$ K is the Debye temperature for Ni [9], one can estimate the coupling constant for Ni to be $G_0 = 18 \times 10^{17}$ W m^{-3} K^{-1}. It should be noted that literature values of the electron–phonon coupling constant for Ni vary in a range from 3.6 to 10.5×10^{17} W m^{-3} K^{-1} [16–18]. As the verification of the value of $\lambda \langle \omega^2 \rangle$ for nonmagnetic Ni is beyond the scope of this paper, and considering that in Ref. [18] the electron–phonon coupling constant of 10.5×10^{17} W m^{-3} K^{-1} is measured in pump-probe reflectivity experiments at relatively low electron temperatures (the transient increase of the electron temperature above the room temperature does not exceed 150 K), we set the coupling factor in Eq. (2) to be equal to 10.5×10^{17} W m^{-3} K^{-1} at $T_e = 300$ K and obtain $\lambda \langle \omega^2 \rangle = 49.5$ meV^2. This value of $\lambda \langle \omega^2 \rangle$ is then used in Eq. (2) to calculate the temperature dependence of the electron–phonon coupling factor in a broad range of temperatures, shown in Fig. 2(d).

As shown in Fig. 2(d), the electron–phonon coupling factor decreases monotonically as the electron temperature increases. The decrease is particularly sharp as the temperature increases up to 3–4×10^3 K and becomes less steep at higher temperatures. As the chemical potential shifts to higher energies (Fig. 2(a)) the contribution of the d band electrons to the electron–phonon coupling decreases. As a result, the electron–phonon coupling factor decreases with respect to its room temperature value by a factor of 4.8 at $T_e = 0.5 \times 10^4$ K, by a factor of 7.1 at $T_e = 1 \times 10^4$ K, and by a factor of 10.5 at $T_e = 2 \times 10^4$ K. The decrease in the strength of the electron–phonon coupling with increasing electronic temperature is consistent with the relative values evaluated in experiments performed at different levels of laser excitation. The highest value of the electron–phonon constant, 10.5×10^{17} W m^{-3} K^{-1}, is obtained from transient

thermoreflectance measurements [18], where the maximum electron temperature increase does not exceed 150 K. Somewhat smaller value of 8×10^{17} W m^{-3} K^{-1} is deduced from pump-probe transmission experiments [17], where the electron temperature increases up to 700 K. Finally, the smallest value of the coupling constant, 3.6×10^{17} W m^{-3} K^{-1}, is obtained by fitting the predictions of the TTM calculations to the threshold fluences for the onset of surface melting [16]. The electron temperature in this case reaches several thousands of Kelvin and the reported value of the effective electron–phonon coupling "constant" is consistent with the temperature dependence shown in Fig. 2(d).

The trend of the temperature dependence of the electron–phonon coupling predicted for Ni in Fig. 2(d) is in apparent contrast with the result predicted for Au [4], where the d band lies ∼2 eV below the Fermi level and, at sufficiently high temperatures, the thermal excitation of d band electrons results in a significant increase of the electron–phonon coupling factor with respect to its room temperature value (by a factor of 5.8 at $T_e = 1 \times 10^4$ K and by a factor of 8.9 at $T_e = 2 \times 10^4$ K). Thus, the neglect of the effect of the thermal excitation of electrons on thermophysical properties of the target material and, in particular, the assumption of a temperature-independent electron–phonon coupling factor, can result, depending on the characteristics of the electron DOS, in either significant overestimation (e.g. Ni) or underestimation (e.g. Au) of the rate of the electron–phonon energy transfer during the time of the electron–phonon equilibration following short pulse laser irradiation.

The theoretical approach used in this work and other studies [2–4] for the calculation of the temperature dependent electron–phonon coupling does not explicitly take into account the umklapp electron–phonon scattering processes [8]. As shown recently by Petrov [19], the umklapp processes make a large contribution to the theoretically predicted values of the electron–phonon coupling. The effect of the umklapp processes on the electron temperature dependence of the electron–phonon coupling, however, is relatively weak for temperatures exceeding the Debye temperature. Since the temperature dependence of the electron–phonon coupling for Ni, shown in Fig. 2(d), is obtained based on the experimental value for the electron–phonon coupling near the room temperature, the contribution from the umklapp processes to the room temperature value of the electron–phonon coupling is implicitly taken into account. As for the temperature dependence of the electron–phonon coupling, the contribution of the umklapp processes [19] is negligible as compared to the contribution from the thermal excitation of d band electrons revealed in this work.

3. TTM results and discussion

Significant deviations of the thermophysical properties of Ni from the commonly used approximations, observed in a range of electron temperatures readily accessible in femtosecond laser material processing applications, may have important practical implications. In order to investigate to what degree the changes in the transient material properties predicted in the previous section

would affect the material response to short pulse laser irradiation, we incorporate the new temperature dependences into TTM model and perform simulations of laser heating and melting of Ni thin films and bulk targets.

Two series of TTM simulations are performed for the same irradiation conditions. In the first series, the commonly used approximations of $C_e = \gamma T_e$ with $\gamma = 1065$ J m^{-3} K^{-2}, $G = 3.6 \times 10^{17}$ W m^{-3} K^{-1} and $K_e = K_0 T_e/T_l$ with $K_0 = 91$ W m^{-1} K^{-1} [9,12,16,20] are used. The value of the coupling constant is chosen to allow for the comparison with earlier simulations and experiments performed for surface melting of Ni films of different thickness [16,20]. In the second series of simulations, the new thermophysical parameters, discussed in Section 2, illustrated in Fig. 2, and given in tabulated form at [11] are used. In both series of TTM simulations, the experimental values of the melting temperature and the latent heat of melting are used, 1728 K and 2.45×10^9 J m^{-3} [21]. The lattice heat capacity, C_l, is obtained by subtracting the electronic contribution from the room temperature value of the total heat capacity, $C_l = C_{total}(300 \text{ K}) - C_e(T_e = 300 \text{ K}) = 3.68 \times 10^6$ J m^{-3} K^{-1}, with $C_{total}(300 \text{ K}) = 4 \times 10^6$ J m^{-3} K^{-1} [21]. The lattice heat capacity is assumed to be constant as the lattice temperature in the TTM calculations reported in this work is either close or higher than the Debye temperature of Ni, 450 K.

3.1. Transient evolution of the electron and lattice temperatures

The evolution of the electron and lattice temperatures at the surface of a bulk Ni target irradiated with a 200 fs laser pulse at an absorbed fluence of 250 J m^{-2} is shown in Fig. 3 for the two sets of thermophysical parameters discussed above. Following
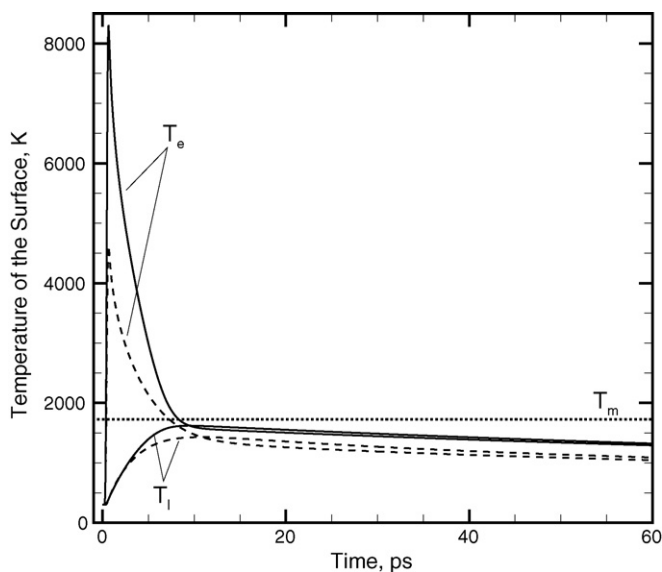
the laser irradiation, the maximum electron temperature achieved by the end of the laser pulse is significantly, by 45%, higher in the model that takes into account the DOS effects on the thermophysical parameters of the material. The observation of the higher maximum electron temperature is directly related to a much weaker increase of the heat capacity with electron temperature as compared to the commonly used linear dependence (Fig. 2(b)).

The evolution of the lattice temperature in the irradiated target is also affected by the choice of the parameters used in the simulations. Despite the weakening of the electron–phonon coupling at high electron temperatures (Fig. 2(d)) the time required for the equilibration between the electrons and the lattice is close in both simulations, ∼10 ps, whereas the maximum lattice temperature achieved at the surface increases by ∼13%, from 1430 to 1620 K, when the modified thermophysical parameters are used. The similarity of the rates of the electron–phonon relaxation can be explained by the larger difference between the lattice and electron temperatures created by the laser excitation predicted with the new set of parameters (Fig. 3) which balances the effect of the weaker coupling at high electron temperatures.

3.2. Fluence threshold for surface melting

To study the effect of the changes in the temperature dependence of thermophysical parameters on the threshold for the onset of surface melting, we perform a series of TTM calculations for Ni films of various thicknesses irradiated with a 200 fs laser pulse. The threshold for surface melting is defined as the fluence at which the lattice temperature at the surface reaches the melting temperature, 1728 K. As shown in Fig. 4, the

Fig. 3. Evolution of the electron and lattice temperatures at the surface of a bulk Ni target irradiated with a 200 fs laser pulse at an absorbed fluence of 250 J m^{-2} predicted in TTM simulations performed with thermophysical parameters calculated with DOS obtained from VASP (solid lines) and the commonly used approximations described in the text (dashed lines). The temperature dependences of thermophysical parameters used in the TTM simulations are shown in Fig. 2.
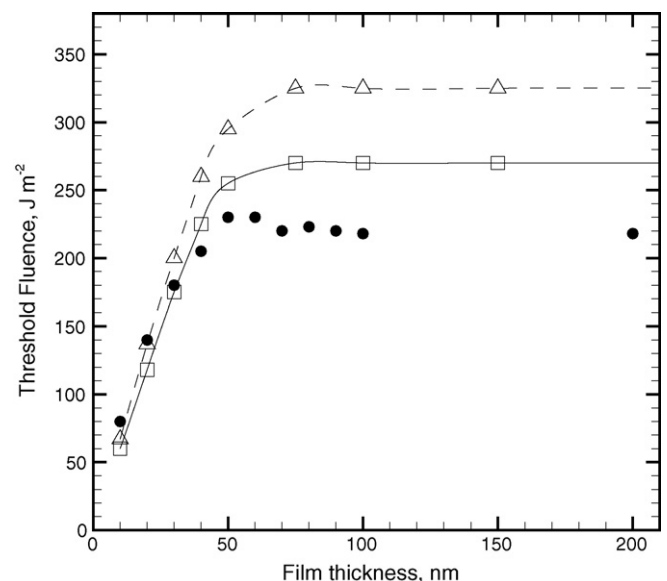

Fig. 4. Threshold fluence for surface melting as a function of film thickness obtained in TTM simulations performed with thermophysical parameters calculated with DOS obtained from VASP (solid lines) and the commonly used approximations described in the text (dashed lines). Experimental data for the melting thresholds from Ref. [16] are shown by filled circles.

experimental threshold fluences [16] and the results obtained in both series of simulations follow the same general trend: linear increase of the threshold fluence with film thickness up to the thickness that corresponds to the diffusive penetration depth of the excited electrons during the time of the electron–phonon equilibration, L_c [16,20], and saturation of the threshold fluence at higher fluences. In a film thinner than L_c, nearly uniform temperature distribution is established by the time of the electron–phonon equilibration and the threshold fluence for melting is defined by the energy density needed to homogeneously heat the film up to the melting temperature. For films thicker than L_c, the electron–phonon equilibration takes place within the electron diffusion length of L_c from the irradiated surface and the threshold fluence for melting becomes independent of thickness. As can be seen from Fig. 4, the values of L_c at the threshold for surface melting are similar, ~ 50 nm, in the two series of TTM simulations, as well as in the experiment.

The saturation threshold fluence at large film thicknesses obtained in the TTM simulations performed with the commonly used parameters, 325 J m^{-2}, is significantly higher than the experimental value, 220 J m^{-2} [16], whereas the value predicted in TTM simulations performed with the new thermophysical parameters, 270 J m^{-2}, is in a better agreement with the experimental data (Fig. 4). As the experimental values are obtained by conversion of multi-shot data to single-shot threshold fluences, further accurate single-shot experimental measurements, along with further improvements of the computational model, are needed to clarify the remaining discrepancy between the experimental and computational values of the laser melting threshold fluences.

4. Summary

The electron temperature dependences of the electron–phonon coupling factor, electron heat capacity and thermal conductivity are investigated for Ni based on the electron DOS obtained from ab initio electronic structure calculations. Due to the presence of large density of states around the Fermi level, thermal excitation of d band electrons leads to a significant decrease in the electron–phonon coupling factor and large negative deviations of the electron heat capacity and the electron thermal conductivity from the commonly used linear dependences on the electron temperature. These large deviations of the thermophysical parameters away from the low temperature values/dependences are predicted for electron temperatures that are commonly realized in ultrashort laser material processing applications and, therefore, can have important practical implications. In particular, TTM simulations performed with the new set of thermophysical parameters predict higher maximum lattice and electron temperatures

achieved at the surface, as well as 17% decrease in the saturation threshold fluence for surface melting of films thicker than 50 nm, as compared to the results obtained using a constant electron–phonon coupling factor and linear temperature dependences of the electron heat capacity and electron thermal conductivity. The new calculated values of the threshold fluences for surface melting are in a better agreement with the results of experimental measurements.

Acknowledgements

References

[1] S.I. Anisimov, B.L. Kapeliovich, T.L. Perel'man, Sov. Phys. JETP 39 (1974) 375.
[2] X.Y. Wang, D.M. Riffe, Y.S. Lee, M.C. Downe, Phys. Rev. B 50 (1994) 8016.
[3] A.N. Smith, P.M. Norris, in: Proceedings of 11th International Heat Transfer Conference, vol. 5, 1998, p. 241.
[4] Z. Lin, L.V. Zhigilei, Proc. SPIE 6261 (2006) 62610U.
[5] T. Tsuchiya, K. Kawamura, Phys. Rev. B 66 (2002) 094115.
[6] (a) G. Kresse, J. Hafner, Phys. Rev. B 47 (1993) 558;
(b) G. Kresse, J. Hafner, Phys. Rev. B 49 (1994) 14251.
[7] G. Kresse, D. Joubert, Phys. Rev. 59 (1999) 1758.
[8] N.W. Ashcroft, N.D. Mermin, Solid State Physics, Holt, Rinehart and Winston, New York, 1976.
[9] American Institute of Physics Handbook, third ed., McGraw-Hill, New York, 1982.
[10] G.K. White, Aust. J. Phys. 46 (1993) 707.
[11] Electron temperature dependences of thermophysical properties of Ni and several other metals are accessible in tabulated form from http://www.faculty.virginia.edu/CompMat/electron-phonon-coupling/.
[12] D.S. Ivanov, L.V. Zhigilei, Phys. Rev. B 68 (2003) 064114.
[13] P.B. Allen, Phys. Rev. Lett. 59 (1987) 1460.
[14] W.L. McMillan, Phys. Rev. 167 (1968) 331.
[15] D.A. Papaconstantopoulos, L.L. Boyer, B.M. Klein, A.R. Williams, V.L. Morruzzi, J.F. Janak, Phys. Rev. B 15 (1977) 4221.
[16] S.-S. Wellershoff, J. Güdde, J. Hohlfeld, J.G. Müller, E. Matthias, Proc. SPIE 3343 (1998) 378.
[17] E. Beaurepaire, J.-C. Merle, A. Daunois, J.-Y. Bigot, Phys. Rev. Lett. 76 (1996) 4250.
[18] A.P. Caffrey, P.E. Hopkins, J.M. Klopf, P.M. Norris, Microscale Thermophys. Eng. 9 (2005) 365.
[19] Yu.V. Petrov, Laser Part. Beams 23 (2005) 283.
[20] D.S. Ivanov, L.V. Zhigilei, Appl. Phys. A: Mater. Sci. Process. 79 (2004) 977.
[21] D.R. Lide (Ed.), CRC Handbook of Chemistry and Physics, 72nd ed., CRC Press, Boca Raton, FL, 1991.